Modeling Zn 2+ Release From Metallothionein

ARTICLE *in* THE JOURNAL OF PHYSICAL CHEMISTRY A · AUGUST 2014

Impact Factor: 2.69 · DOI: 10.1021/jp503189v · Source: PubMed

4 AUTHORS, INCLUDING:

Todor Dudev

Academia Sinica

45 PUBLICATIONS **1,664** CITATIONS

SEE PROFILE

Carmay Lim

Academia Sinica

144 PUBLICATIONS **4,086** CITATIONS

SEE PROFILE

THE JOURNAL OF PHYSICAL CHEMISTRY A

Article

pubs.acs.org/JPCA

Modeling Zn^{2+} Release From Metallothionein

C. Satheesan Babu,[†,∥] Yu-Ming Lee,[†,∥] Todor Dudev,[†,§] and Carmay Lim*[,†,‡]

[†]Institute of Biomedical Sciences, Academia Sinica, Taipei 115, Taiwan, R.O.C.

[‡]Department of Chemistry, National Tsing Hua University, Hsinchu 300 Taiwan, R.O.C.

Supporting Information

ABSTRACT: Mammalian metallothioneins (MTs) comprise a Zn_3Cys_9 cluster in the β domain and a Zn_4Cys_{11} cluster in the α domain. They play a crucial role in storing and donating Zn^{2+} ions to target metalloproteins and have been implicated in several diseases, thus understanding how MTs release Zn^{2+} is of widespread interest. In this work, we present a strategy to compute the free energy for releasing Zn^{2+} from MTs using a combination of classical molecular dynamics (MD) simulations, quantum-mechanics/molecular-mechanics (QM/MM) minimizations, and continuum dielectric calculations. The methodology is shown to reproduce the experimental observations that (1) the Zn-binding sites do not have equal Zn^{2+} affinity and (2) the isolated β domain is thermodynamically less stable and releases Zn^{2+} faster with oxidizing agents than the isolated α domain. It was used to compute the free energies for Zn^{2+} release from the metal cluster in the absence and presence of the protein matrix (protein architecture and coupled protein−water interactions) to yield the respective disulfide-bonded product. The results show the importance of the protein matrix as well as protein dynamics and coupled conformational changes in accounting for the differential Zn^{2+}-releasing propensity of the two domains with oxidizing agents.

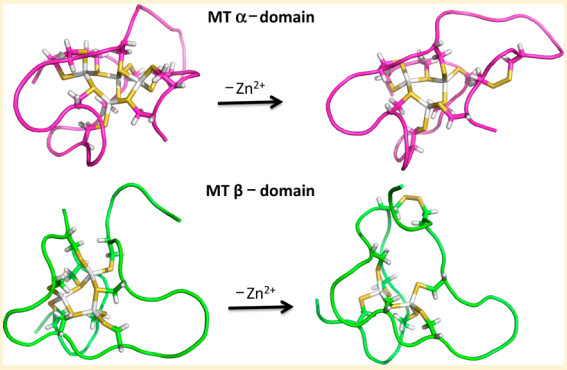

INTRODUCTION

Metallothioneins (MTs) are a family of low-molecular weight, cysteine-rich, and metal-rich proteins present in all living organisms.[1,2] In mammals, four MT isoforms designated MT-1, MT-2, MT-3, and MT-4 are found in different organs. MT-1 and MT-2 are widely expressed isoforms in metabolic systems such as liver and kidney,[3,4] MT-3 is predominant in the central nervous system,[5] whereas MT-4 is mainly distributed in certain squamous epithelial cells.[6,7] MT-1 and MT-2 bind predominantly Zn^{2+}, and to a lesser extent Cd^{2+} and a few other heavy metal ions, whereas MT-3 prefers equally Zn^{2+} and copper ions.[8] Depending on the organism and/or isoforms, MTs function in transport, storage, and concentration regulation of physiologically essential metal ions, control of neuronal growth, as well as protection against heavy metal toxicity and reactive oxygen species.[9−15] Notably, MTs maintain the free intracellular Zn^{2+} concentration in the picomolar range,[16,17] supplying Zn^{2+} to several enzymes such as carbonic anhydrase, glycerol phosphate dehydrogenase, carboxypeptidase A, sorbitol dehydrogenase, and alkaline phosphatase, and exchange Zn^{2+} with Zn fingers.[18−20] Because MTs have multiple biological functions, they have been implicated in immune defense responses, regulation of DNA binding and gene expression, mitochondrial function and energetic metabolism, angiogenesis, cell proliferation and differentiation, signal transduction, and apoptosis.[21,22] In some circumstances, MTs have adverse effects on human health: They are overexpressed in various human tumors[23,24] and may contribute to drug resistance because MTs can bind Pt^{2+} in cisplatin, a chemotherapy agent.[25,26] Mammalian MT-1, MT-2, and MT-3 have been implicated in neurodegenerative diseases such as Alzheimer's disease, amyotrophic lateral sclerosis, and multiple sclerosis, as well as multiple stress-induced inflammatory processes.[21,27,28] On the other hand, they can serve as neuroprotective agents for cerebral ischemia and seizure.[21] Because of the biological importance of mammalian MTs and its role in various diseases,[29−31] MTs are of great interest to study.

The four mammalian MT isoforms consist of 61−68 residues, 20 of which are Cys residues comprising a N-terminal β domain and a C-terminal α domain. Under physiological conditions, vertebrate MTs bind Zn^{2+} and form a Zn_3Cys_9 cluster in the β domain (Figure 1a) and a Zn_4Cys_{11} cluster in the α domain (Figure 1b). The Cys S atom binds a single Zn^{2+} (terminal S^t) or bridges two Zn^{2+} (bridging S^b). In the N-terminal β domain, the three Zn^{2+} have the same set of first-shell ligands: each Zn^{2+} is bound to two terminal S^t and two bridging S^b atoms. In the C-terminal α domain, two of the Zn^{2+} have the same first-shell ligands as the Zn^{2+} in the β domain, but the other two Zn^{2+} are bound to only one S^t and three S^b

Special Issue: International Conference on Theoretical and High Performance Computational Chemistry Symposium

Received: March 31, 2014
Revised: August 12, 2014
Published: August 13, 2014

   dx.doi.org/10.1021/jp503189v | J. Phys. Chem. A 2014, 118, 9244−9252

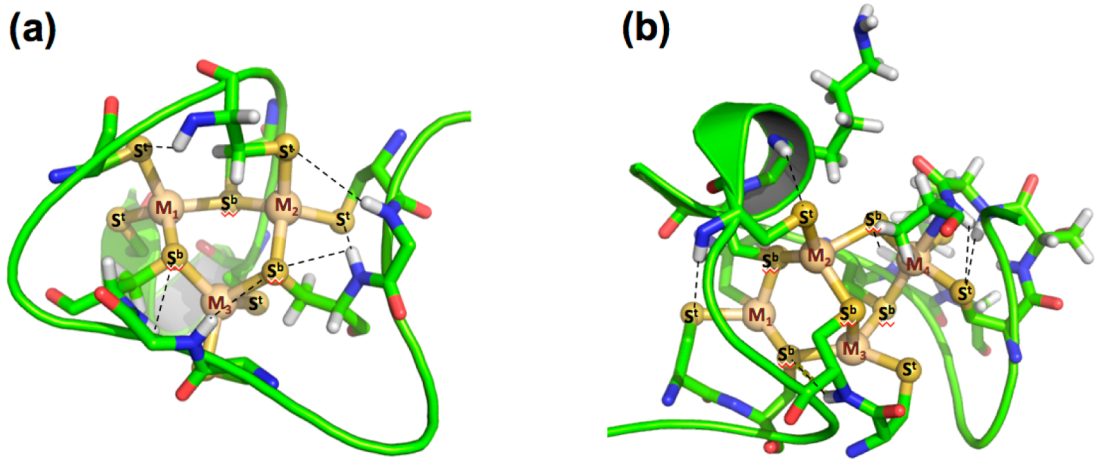

Figure 1. Individual structures of human MT-2 (a) β domain (PDB code: 1MHU) and (b) α domain (PDB code: 2MHU).

Scheme 1. Oxidation of the MT (A) α and (B) β Domain with the Concomitant Release of Zn^{2+} and Formation of a Disulfide Bond[a]

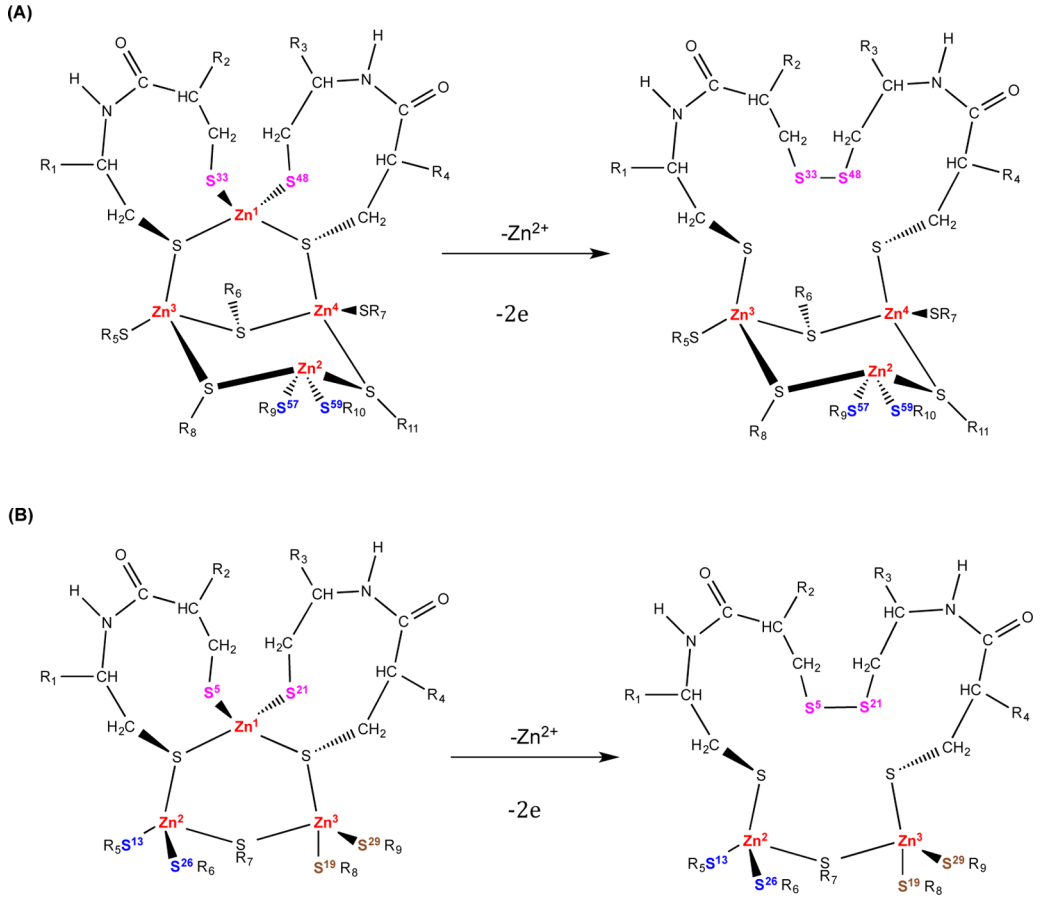

[a] S^i denotes the sulphur belonging to Cys *i*.

atoms. Thus, the number of Zn−S^b bonds per metal in the α domain is greater than that in the β domain. Hydrogen bonds between the backbone amide and the Zn-bound thiolates are commonly observed in the 3D structures of the β and/or α domain of the MTs.[31−38]

Although MTs were discovered more than 50 years ago, MTs remain enigmatic because of their promiscuous functions and peculiar reactivity in the individual clusters. Compared to the Zn_4Cys_{11} cluster in the isolated α domain, the Zn_3Cys_9 cluster in the β domain is less stable and releases Zn^{2+} faster with 5,5′-dithio-*bis*(2-nitrobenzoic acid) (Ellman's reagent), but it is more stable toward Zn^{2+}-chelating agents.[33] The higher stability of the α domain has been attributed to its greater number of bridging bonds compared to the β domain.[33] On the other hand, density functional theory (DFT) calculations of the isolated metal clusters[39] as well as human MT-2 β and α domains[40] have attributed the higher reactivity of the β domain to its smaller volume: Although the net charge of both metal

dx.doi.org/10.1021/jp503189v | J. Phys. Chem. A 2014, 118, 9244−9252

clusters is −3e, it is less dispersed in the smaller β domain, resulting in Zn−S^b and Zn−S^t bonds (2.44 and 2.37 Å) that are longer than those in the α-domain (2.40 and 2.36 Å).[40] The mPW1PW91 functional with the 6-311+G(d,p) basis set for the Zn cluster and the semiempirical PM6 method for the protein has been used to study thiolate reactivity with hydrogen peroxide with concomitant Zn^{2+} release from the β domain, but not from the α domain.[41] Although molecular dynamics (MD) and molecular mechanics calculations in vacuum have shown that the number of hydrogen bonds in both domains increases upon sequential metal release via protonation of the cysteinyl sulfurs,[42] the difference between the β and α domains in releasing Zn^{2+} has not been investigated. Other simulation studies have focused on the structures and dynamics of the individual domains from various isoforms.[43−45]

The aforementioned explanations for the enhanced reactivity of the β domain compared to the α domain are based only on the β and α domain structures, but not on the corresponding Zn-released product structures. Although MD simulations can sample the Zn-released product configurations efficiently, they yield inaccurate metal cluster structures if conventional force fields that do not account for significant charge transfer and polarization effects of the Zn clusters are employed.[46−48] On the other hand, DFT calculations become inefficient and prohibitive in sampling the conformational space of the Zn-released product. While a high level of theory for the reacting metal cluster and a semiempirical level for the protein environment have been used to compute the energy barrier upon thiolate reaction with hydrogen peroxide in the MT-2 β domain,[41] conformational and dynamical effects have been assumed to be negligible. To our knowledge, no study has computed the free energy of Zn^{2+} release from both MT domains in aqueous solution.

The aim of this work is to present a strategy to compute the free energy for Zn^{2+} release from MTs. Since reactivation of metal-free sorbital dehydrogenase requires a 1:1 molar ratio of MT, indicating that only one of the seven MT Zn^{2+} is transferred,[1] and the stability constant of one of the seven MT Zn^{2+} is significantly smaller than the other six,[49] we assume that MT releases one Zn^{2+} first, rather than all seven Zn^{2+} at once. Most oxidizing agents oxidize thiolates in MT to disulfides with the release of Zn^{2+} (see Scheme 1).[50,51] Hence, the free energy for Zn^{2+} release from each MT domain was computed as the free energy difference between the disulfide-bonded product and the corresponding reactant using a combination of classical MD simulations, quantum-mechanics/molecular-mechanics (QM/MM) energy minimizations and continuum dielectric calculations. The methodology was tested to see if it could reproduce the experimental observation that the Zn_3Cys_9 cluster in the isolated β domain is less stable and releases Zn^{2+} faster with Ellman's reagent than the Zn_4Cys_{11} cluster in the corresponding α domain.[33] The results show the importance of the protein dynamics and coupled conformational changes as well as the protein matrix in accounting for the differential Zn^{2+}-releasing propensity of the two domains upon reaction with oxidizing agents. The computational strategy presented herein is not limited to MT but can be extended to study metal release from other metalloproteins.

METHODS

Calibration of Geometry Optimization Method. To determine a suitable quantum mechanical (QM) method for optimizing the MT α and β domain geometries, the Cambridge Structural Database (CSD)[52] was searched for high-resolution X-ray structures of polynuclear Zn complexes mimicking the multimetal binding cores of MT. The compound that most resembled the MT Zn_3Cys_9 or Zn_4Cys_{11} core is the $[Zn_2(SC_2H_5)_6]^{2-}$ complex (CSD entry DETHUF, Supplementary Figure S1, Supporting Information), whose structure had been refined to a conventional R value of 4%.[53] This molecule was fully optimized using four density functionals with five types of basis sets using the Gaussian 09[54] program. The SVWN, BP86, B3LYP, and TPSSH functionals with the SDD, SVP, TZVPP, 6-31+G(d), and 6-31++G(d,p) basis sets were chosen for testing since they had been used in previous studies to optimize Zn complexes.[39,40,55−57] The S-VWN/SDD method most efficiently reproduced the geometry seen in the high-resolution X-ray structure of the $[Zn_2{\cdot}(SC_2H_5)_6]^{2-}$ complex. It yielded mean Zn−S^b (2.410 Å) and Zn−S^t (2.306 Å) distances as well as Zn−S−Zn (81.7°) and S−Zn−S (98.1°) angles that agree with the respective CSD values to within experimental and computational error (Supplementary Table S1). It was further calibrated by assessing its ability to predict the MT Zn_3Cys_9 and Zn_4Cys_{11} structures (see Results).

Reaction Modeled. We modeled Zn^{2+} release from the solvated MT domains upon oxidation with Ellman's reagent yielding various disulfide products.[50,51] In the β domain, release of each of the three Zn^{2+} bound to two S^t and two S^b atoms yielded three products designated by the disulfide bridge formed (C^5−C^{21}, C^{13}−C^{26}, and C^{19}−C^{29}, Scheme 1b). In the α domain, release of each of the two Zn^{2+} with the same metal ligands as the Zn^{2+} in the β cluster yielded two products (C^{33}−C^{48} and C^{57}−C^{59}, Scheme 1a). Release of the other two Zn^{2+} in the α domain, which are bound to one S^t and three S^b atoms, would convert the S^b to S^t atoms after Zn^{2+} release rather than forming a disulfide bond. We also modeled Zn^{2+} release from isolated $Zn_4(MeS)_{11}$ or $Zn_3(MeS)_9$ clusters in solution with MeS modeling the Cys side chain.

MD Simulations. A total of seven 22 ns MD simulations were performed for the β domain (1 reactant and three products) and α domain (1 reactant and two products). The MD simulations for each reactant and corresponding Zn^{2+}-released product in aqueous solution were performed using the CHARMM37[58] program at physiological pH and a mean temperature of 300 K and 1 atm.

Force Field. The MD simulations employed the all-hydrogen CHARMM27 force field for the protein atoms,[59] the TIP3P[60] model for the water molecules, and periodic boundary conditions. The ion−water interaction energies were modeled by a sum of Coulomb and vdW pairwise energies using vdW parameters that have been constructed to reproduce the experimentally observed ion−water distance, hydration number, and hydration free energy of Zn^{2+}.[47] All bonds involving hydrogen atoms were constrained during the simulations using the SHAKE algorithm.[61] The vdW interactions employed a group-based cutoff at 13 Å with a switching function in the region from 11 to 13 Å, while the long-ranged electrostatic interactions were treated using the particle-mesh Ewald method.[62] The nonbonded interactions were updated heuristically using a 14-Å cutoff.

Starting Reactant Structures. The starting structure for the simulation of the MT domains is the 2-Å X-ray structure of rat MT-2 (PDB entry 4MT2) with the Cd^{2+} ions replaced by Zn^{2+}. The first 31 residues of MT-2 comprise the β domain, while the remaining residues comprise the α domain. Hydrogen atoms were added to the all-Zn^{2+} crystal structure, and their positions

dx.doi.org/10.1021/jp503189v | J. Phys. Chem. A 2014, 118, 9244−9252

were energy minimized to remove bad contacts. To account for differences between the Cd−S and Zn−S distances, the three-Zn^{2+} and four-Zn^{2+} structures were energy minimized by QM/MM in the field of fixed MM charges (see next section). The resulting structures of the β and α domains were solvated in a pre-equilibrated cubic box of edge length 35 Å containing TIP3P water molecules. Water molecules within 2.5 Å of any of the heavy atoms were removed, resulting in 1324 and 1338 water molecules for the β and α domains, respectively. To ensure charge neutrality for the particle-mesh Ewald calculations, a bulk water molecule was replaced by a Zn^{2+} in the α domain and its position was re-equilibrated, whereas this was not needed for the β domain, which was already neutral.

Simulation Protocol. The solvated MT domain was energy minimized, initially by fixing the backbone atoms, the Zn^{2+} ions, and the Cys side chains, and later releasing the constraints on the backbone atoms. The solvated system was then equilibrated and subjected to production dynamics for a nanosecond using a time step of two femtoseconds. As the classical force field used neglects charge transfer and polarization effects, the Zn^{2+} ions and the Cys side chains were fixed throughout the simulation. The temperature and pressure were maintained using a coupling bath. The configuration of the β or α domain after 1 ns was subjected to QM/MM energy minimizations (see below) and electrostatic potential (ESP)[63] charges for the metal ions and ligands were computed. Using these charges, the new positions of the Zn^{2+} ions and thiolates were again frozen, and another 1 ns MD trajectory was generated. This was repeated to yield four 1 ns trajectories. After 4 ns, the simulation was continued for another 18 ns for a total of 22 ns with the Zn^{2+} ions and the Cys side chains fixed using ESP charges for the metal ions and ligands derived from the QM/MM energy-minimized structure at 4 ns.

For the product, each Zn^{2+} ion was in turn removed from the final configuration of the first 1 ns trajectory, and a disulfide bond was formed between the two terminal S^t atoms. Each Zn^{2+}-released product was subjected to energy minimization followed by a short re-equilibration. The same simulation procedure used for the reactant was followed for each product to generate four 1 ns trajectories and one 18 ns trajectory for a total length of 22 ns.

QM/MM Minimizations. The Zn^{2+} ions and the Zn^{2+}-bound Cys side chains were treated using the calibrated S-VWN/SDD method to account for charge transfer and polarization effects. The QM subsystem consists of three Zn^{2+} ions and the nine thiolate groups for the β domain and four Zn^{2+} ions and 11 thiolates for the α domain. The QM subsystem for the product differs from that for the reactant in that the number of Zn^{2+} ions in each domain is reduced by one and the terminal S^t atoms that were originally bound to the released Zn^{2+} formed a disulfide bridge. The QM subsystem was connected to the MM region using hypothetical H atoms to link the C^α and C^β atoms of all the metal-bound cysteines. The final configuration from each 1 ns trajectory was relaxed by SVWN-SDD/MM energy minimizations using the Gaussian09 program link[64,65] in the CHARMM37[58] program. To speed up convergence, the solvent and the protein part of the configuration was frozen, and the QM subsystem was energy-minimized in the field of fixed MM charges. Based on the QM/MM energy-minimized structure, ESP charges[63] on the QM atoms were obtained.

Free Energy Calculations. Thirty-six configurations from every 0.5 ns of the 4.5−22 ns segment of each MD trajectory were SVWN-SDD/MM energy minimized and used to compute the free energy of Zn^{2+} release (ΔG^{80}) according to Scheme 2, where ε = 1 represents vacuum and ε = 80 corresponds to the dielectric constant of water. The ΔG^1 was estimated by the difference in the QM/MM energies of the Zn-released product relative to the corresponding Zn-loaded domain:

Scheme 2

$$\begin{array}{ccc} & \xrightarrow{\Delta G^1} & \\ [\text{Reactants}]\ (\varepsilon = 1) & \rightarrow & [\text{Products}]\ (\varepsilon = 1) \\ \Delta G_{solv}\ (\text{Reactants})\ \downarrow & & \downarrow\ \Delta G_{solv}\ (\text{Products}) \\ [\text{Reactants}]\ (\varepsilon = 80) & \rightarrow & [\text{Products}]\ (\varepsilon = 80) \\ & \xrightarrow{\Delta G^{80}} & \end{array}$$

$$\Delta G^1 \sim \Delta E_{QM/MM} = E_{QM/MM}(\text{Products}) - E_{QM/MM}(\text{Reactants}) \quad (1)$$

Based on the SVWN-SDD/MM energy-minimized geometries, the QM/MM energies were estimated by single point calculations at the B3LYP/6-311++G(2d,2p) level in the field of fixed water and protein charges. The B3LYP/6-311++G(2d,2p) method was chosen, as it can reproduce the experimental gas-phase deprotonation free energies of H_2S and has been successfully used in metal-induced Zn-finger folding calculations.[66] The solvation free energy, ΔG_{solv}, was approximated as a sum of the electrostatic (ΔG_{solv}^{elec}) and nonelectrostatic ($\Delta G_{solv}^{nonelec}$) terms; i.e., $\Delta G_{solv} \sim \Delta G_{solv}^{elec} + \Delta G_{solv}^{nonelec}$. The electrostatic contribution, ΔG_{solv}^{elec}, was estimated by solving the Poisson equation using the ESP charges derived from the QM/MM energy-minimized structures and atomic radii parameters optimized for Poisson−Boltzmann calculations in the CHARMM force field.[67] The nonelectrostatic contribution, $\Delta G_{solv}^{nonelec}$, was approximated by a linear function of the solvent accessible surface area (SASA); i.e., $\Delta G_{solv}^{nonelec} \sim \gamma \times \text{SASA} + 0.92$, with γ equal to 5.42 cal/mol/Å^2.[68] Thus, the free energy of Zn^{2+} release was computed as a sum of the QM/MM energy and the solvation free energy change for the reaction; i.e.,

$$\Delta G^{80} = \Delta G^1 + \Delta\Delta G_{solv} \sim \Delta E_{QM/MM} + \Delta\Delta G_{solv}^{elec} + \Delta\Delta G_{solv}^{nonelec} \quad (2)$$

RESULTS

Calibration of the S-VWN/SDD β and α Geometries. To verify the reliability of the S-VWN/SDD method for optimizing the MT geometries, it was used to predict the geometries of the α and β metal clusters in MT, whose initial geometries were taken from the 2.0 Å X-ray structure of rat MT-2 (PDB code: 4MT2). Models ***β*-MT′** (Figure 2a) and ***α*-MT′** (Figure 2b) included all backbone peptide groups and the Cys side chains, but the side chains of the other amino acid residues were replaced by hydrogen atoms. The S-VWN/SDD optimized structure preserved the NH···S hydrogen bonds observed in the crystal structure. Because the α domain contains four Cd^{2+}, but the β domain contains two Zn^{2+} and one Cd^{2+} in the 4MT2 structure, the fully optimized S-VWN/SDD geometry of ***β*-MT′** was compared with the crystal structure. The S-VWN/SDD method could reproduce the β

dx.doi.org/10.1021/jp503189v | J. Phys. Chem. A 2014, 118, 9244−9252

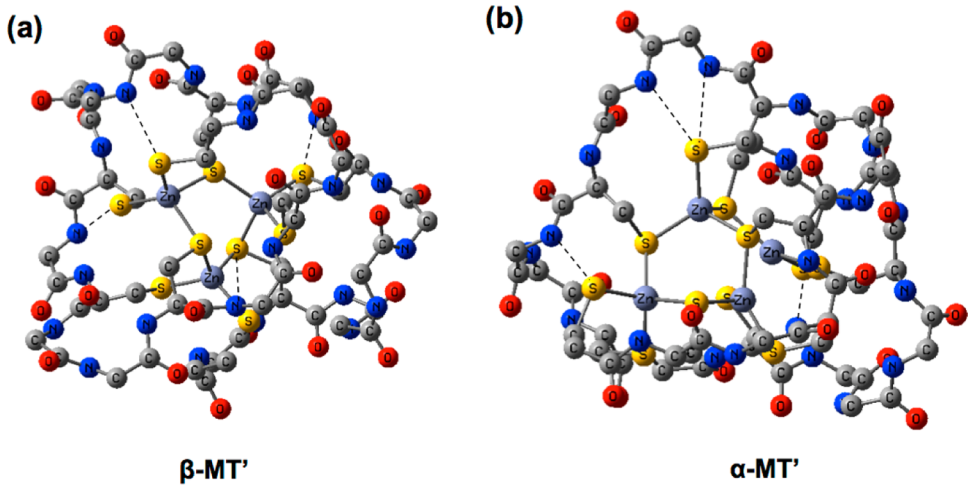

Figure 2. Fully optimized S-VWN/SDD geometries of models of (a) MT-2 β domain and (b) MT-2 α domain. Dashed lines denote conserved NH···S hydrogen bonds.

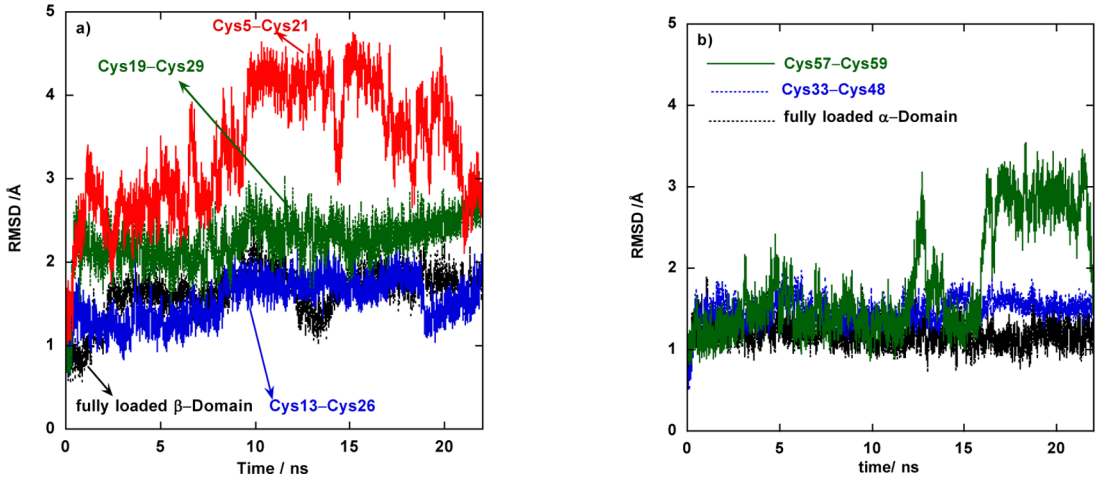

Figure 3. Backbone RMSDs as a function of the simulation time in the MT-2 (a) β domain and (b) α domain and their respective Zn-released products, which are labeled by the disulfide bond formed.

domain geometry seen in the X-ray structure: The average Zn−S^t (2.32 Å) and Zn−S^b (2.38 Å) distances in the fully optimized structure of the ***β*-MT′** model agree with those in the 4MT2 structure of the β domain (2.36 and 2.40 Å) to within experimental error. They are close to the average Zn−S^t and Zn−S^b distances in the fully optimized ***α*-MT′** structure (2.35 and 2.36 Å).

Calibration of the MD Simulations. From the 4−22 ns segment of each trajectory, the root-mean-square deviations (RMSDs) of the backbone N, C^α, and C atoms in the MD structures of the Zn-loaded domains from those in the respective energy-minimized X−ray structures were computed. Furthermore, the 4−22 ns segment of each trajectory was analyzed for hydrogen bonds, defined by a H to acceptor distance $\leq$ 2.75 Å and an acceptor−H−donor angle $\geq$ 120°. The MD simulations could maintain the structural integrity of the X-ray structure: The backbone RMSDs for the β (Figure 3a) and α (Figure 3b) domains, which plateaued around 1.5 and 1.25 Å respectively, were below those in 10 NMR conformers of the rat MT-2 β (2.4 Å) and α (1.9 Å) domain from the respective X-ray structure.[32] Both sets of RMSDs indicate that the β domain is more flexible than the α domain.

The MD simulations could also maintain hydrogen bonds seen in the crystal structure: All hydrogen bonds seen in the β domain of the 4MT2 structure were present in the isolated β domain simulation except the hydrogen bonds with the terminal residues (Met 1 and Lys31), whereas the S18 N··· A16 O and K30 N^Z···C20 O hydrogen bonds were replaced by S18 N···C15 O and K30 N···C26 O hydrogen bonds, respectively, in the simulation (Supplementary Table S2a). In addition, A16 N···C15 S^t and K25 N^Z···D2 O^D hydrogen bonds were present for over 75% of the time during the 18 ns simulation. Likewise, all hydrogen bonds seen in the α domain of the 4MT2 structure were present in the α domain simulation except those with the N-terminal S32 and K56 residues, while the C41 amide hydrogen bonds to the backbone O of V39 instead of P38, as found in the crystal structure (Supplementary Table S2b). A stable C44 N···C41 S^t hydrogen bond was also formed in the α simulation. The hydrogen bond differences between the crystal structure and simulations may be because (i) the 4MT2 structure contains four Cd^{2+} in the α domain and one Cd^{2+} in the β domain, and (ii) the simulations were performed for the separate domains rather than the entire molecule.

dx.doi.org/10.1021/jp503189v | J. Phys. Chem. A 2014, 118, 9244−9252

Table 1. Relative QM/MM Energies, Solvation and Solution Free Energies (in kcal/mol) for Releasing a Zn^{2+} Ion from the β and α Domain[a]

reactant	product	$\Delta\Delta G^{80}$,[b] kcal/mol	$\Delta\Delta E_{QM/MM}$[c] kcal/mol	$\Delta\Delta\Delta G_{solv}^{elec}$,[d] kcal/mol	$\Delta\Delta\Delta G_{solv}^{nonelec}$,[e] kcal/mol
$[MT-\alpha]^{2-}$	$C^{57}-C^{59}$	0.0	0	0	0
	$C^{33}-C^{48}$	−14.1	−39.6	26.5	−1.0
$[MT-\beta]^{0}$	$C^{5}-C^{21}$	−18.4	−34.5	15.1	1.0
	$C^{13}-C^{26}$	−25.6	−54.3	29.2	−0.5
	$C^{19}-C^{29}$	−37.1	−36.0	−0.9	−0.2

[a]All energies and free energies were computed relative to those for releasing a Zn^{2+} from the α domain to generate the $C^{57}-C^{59}$ product. [b]$\Delta\Delta G^{80}$ is the relative solution free energy for releasing a Zn^{2+} ion. [c]$\Delta\Delta E_{QM/MM}$ is the relative QM/MM energy for releasing a Zn^{2+}, estimated by single point calculations at the B3LYP/6-311++G(2d,2p) level in the field of fixed water and protein charges based on SVWN-SDD/MM energy-minimized geometries. [d]$\Delta\Delta\Delta G_{solv}^{elec}$ is the relative electrostatic solvation free energy difference between the products and reactants. [e]$\Delta\Delta\Delta G_{solv}^{nonelec}$ is the relative *non*-electrostatic solvation free energy difference between the products and reactants.

Calibration of the Zn-Release Free Energies. To test the strategy used to compute the Zn^{2+}-release free energy, we assessed its ability to reproduce the following experimental observations: (1) All seven metal-binding sites do not have equal affinity for Zn^{2+}.[18] (2) Compared to the isolated α domain, the β domain is thermodynamically less stable and releases Zn^{2+} faster with Ellman's reagent to yield disulfide products.[33] Release of each of the three Zn^{2+} in the β domain yielded three disulfide products ($C^{5}-C^{21}$, $C^{13}-C^{26}$, and $C^{19}-C^{29}$), whereas release of each of the two Zn^{2+} in the α domain with the same first-shell ligands as the Zn^{2+} in the β cluster yielded two products ($C^{33}-C^{48}$ and $C^{57}-C^{59}$). The QM/MM energies, electrostatic solvation free energies, and solvent accessible surface areas for each of the 36 configurations from the 4.5−22 ns MD trajectories of the β or α reactant and product states are listed in Supplementary Tables S3a and S3b along with their standard deviations. These were used to compute the Zn^{2+}-release free energy ΔG^{80} according to eq 2. To maximize error cancellation, the Zn^{2+}-release free energy corresponding to a given $C^{i}-C^{j}$ product was computed relative to the free energy for releasing Zn^{2+} from the α domain to yield the $C^{57}-C^{59}$ product.

The relative free energies in Table 1 could reproduce the above experimental observations: The five Zn^{2+} ions, which are each bound to two terminal S^{t} and two bridging S^{b} atoms, are released with different $\Delta\Delta G^{80}$ free energies despite their similar coordination environments. Furthermore, Zn^{2+} release from the β domain is thermodynamically more favorable than that from the α domain: the ΔG^{80} free energy for releasing Zn^{2+} from the β domain yielding the $C^{5}-C^{21}$, $C^{13}-C^{26}$, or $C^{19}-C^{29}$ product is more favorable than that for releasing Zn^{2+} from the α domain yielding the $C^{33}-C^{48}$ or $C^{57}-C^{59}$ product. However, in the MD simulation of the β domain, the S atoms of C5 and C21 are buried with a combined SASA < 5 $Å^2$, so they may not be accessible to an oxidizing agent unlike the S atoms of C13, C26, C19 and C29, which are solvent exposed.

Differential Solvation Effects Facilitate Zn^{2+} Release from the β domain to Form Disulfide Products. To elucidate why Zn^{2+} release from the β domain is more favorable than Zn^{2+} release from the α domain, the relative free energy for releasing Zn^{2+} in aqueous solution, ΔG^{80}, was decomposed into its constituent QM/MM energy change ($\Delta\Delta E_{QM/MM}$) and solvation free energy change ($\Delta\Delta\Delta G_{solv}$). The results in Table 1 show that solvation by the protein matrix (protein excluding the metal cluster and coupled protein−water interactions) and bulk water both favor Zn^{2+} release from the β domain to form disulfide products. Formation of the $C^{13}-C^{26}$ β product ($\Delta\Delta E_{QM/MM}$ = −54 kcal/mol) is more favorable than formation of the $C^{33}-C^{48}$ α product ($\Delta\Delta E_{QM/MM}$ = −40 kcal/mol) due mainly to protein environment and coupled protein−water interactions stabilizing the metal cluster, as the bulk solvation effects ($\Delta\Delta\Delta G_{solv}$) of these two products are similar. On the other hand, formation of the $C^{5}-C^{21}$ or $C^{19}-C^{29}$ β products is more favorable than formation of the $C^{33}-C^{48}$ α product probably because these two β products underwent conformational changes resulting in a solvation free energy gain. Indeed, the backbone RMSD time-series of the $C^{5}-C^{21}$ or $C^{19}-C^{29}$ β product deviate from that of the β reactant (Figure 3a), whereas the backbone RMSD time-series of the $C^{33}-C^{48}$ α product mimicked that of the α reactant (Figure 3b).

Zinc Release from Isolated α and β Clusters. To assess the contributions from the protein matrix in enabling Zn^{2+} release from the MT domain, we computed the average free energies of releasing each Zn^{2+} bound to two terminal S^{t} atoms and two bridging S^{b} atoms from the isolated $Zn_3(MeS)_9$ and $Zn_4(MeS)_{11}$ clusters using eqs 1 and 2 (see Methods). The mean free energy for releasing a Zn^{2+} from the $Zn_3(MeS)_9$ cluster was computed relative to the corresponding value for the $Zn_4(MeS)_{11}$ cluster. In the absence of the protein matrix and bulk solvent, Zn^{2+} release from the three-Zn^{2+} β cluster becomes less favorable than that from the four-Zn^{2+} α cluster ($\Delta\Delta E_{QM/MM}$ = 3.6 kcal/mol). This is probably because Zn^{2+} release from the α cluster yields a stable six-membered ring containing three Zn^{2+} and three bridging S^{b} atoms (see Scheme 1A). Bulk solvation effects slightly favor Zn^{2+} release from the β cluster ($\Delta\Delta\Delta G_{solv}$ = −1.8 kcal/mol), reducing the free energy difference between Zn^{2+} release from the *solvated* α and β clusters ($\Delta\Delta G^{80}$ = 1.7 kcal/mol).

■ CONCLUDING DISCUSSION

This work presents a computational strategy to calculate the free energy for Zn^{2+} release from MTs. The calculations could reproduce two important experimentally observed features: (i) the metal-binding sites display variable Zn^{2+} affinity, and (ii) the isolated β domain is less stable toward Ellman's reagent than the isolated α domain.[33] This nontrivial successful calibration is because the computational strategy used in modeling Zn^{2+} release included explicit treatment of electronic (charge transfer and polarization) effects, protein matrix and protein dynamical (e.g., conformational changes in product states) effects, as well as bulk solvent effects. The strategy presented can be used to design calculations to elucidate how MTs, which play important roles in inflammatory and neurodegenerative diseases, function as metal buffers and metal transfer proteins. It can also be used to study Zn^{2+} release

dx.doi.org/10.1021/jp503189v | J. Phys. Chem. A 2014, 118, 9244−9252

from other Zn^{2+} proteins such as Zn fingers and Zn-dependent enzymes.

This work also shows that the S-VWN/SDD method can be used for geometry optimization of polynuclear Zn-sites, as it yields average Zn−S distances for the $[Zn_2{\cdot}(SC_2H_5)_6]^{2-}$ complex in excellent agreement with the CSD structure (see Supplementary Table S1). It could also reproduce the Zn−S distances in X-ray structures of MT to within experimental error (Table 1). This is consistent with previous works,[69−71] in which the S-VWN functional[72] and the SDD basis set[73] were shown to be adequate for reproducing bond distances such as Zn−N and Zn−S in mononuclear Zn complexes to within experimental error.

Properties Responsible for the Different Zn-releasing Propensities. Interestingly, although the three Zn^{2+} ions in the β domain and two of the Zn^{2+} ions in the α domain are each bound to two terminal S^t and two bridging S^b atoms, their release results in different free energies in aqueous solution. In the absence of the protein matrix, the solution free energies for releasing Zn^{2+} bound to two S^t and two S^b atoms in the isolated metal clusters are similar (see above). Thus, the protein matrix makes each metal site distinct with different Zn^{2+} dissociation propensities. It also dictates the accessibility of the cysteines to oxidizing agents, as manifested by the fact that the C19 and C29 S atoms are solvent exposed in the isolated β domain, but are buried in the presence of the α domain in the 4MT2 structure. In addition to the protein matrix, differential flexibility of the products resulting in different bulk solvation effects also accounts for the different Zn^{2+}-releasing propensities, as the C^5−C^{21} and C^{19}−C^{29} β products have similar $\Delta E_{QM/MM}$ energies but quite different $\Delta\Delta G_{solv}$ free energies (Table 1).

Physical Basis for the Differential Zn-releasing Propensities of the α and β MT Domains. The calculations suggest that differences in solvation by the protein matrix and bulk water favor Zn^{2+} release from the β domain rather than the α domain to form disulfide products; as in the absence of the protein matrix and bulk water, Zn^{2+} release from the four-Zn^{2+} α cluster, which yields a stable six-membered ring, is favored over that from the three-Zn^{2+} β cluster (see above). The protein matrix induces these differential Zn^{2+}-releasing propensities owing to differences in hydrogen-bonding interactions, conformational fluctuations, and solvation of the Zn-released product structures. Notably, the C^{19}−C^{29} β product has more flexibility to undergo conformational changes than the C^{33}−C^{48} α product (Figure 3), resulting in better solvation (see Table 1).

The calculations also suggest a plausible reason why the Zn_3Cys_9 cluster in the β domain is more stable toward Zn^{2+}-chelating agents than the Zn_4Cys_{11} cluster in the α domain.[33] Unlike oxidizing agents, Zn^{2+}-chelating agents destroy the native structure of the protein surrounding the β or α metal cluster; hence the Zn-releasing propensity would likely depend on the intrinsic reactivity of the isolated metal clusters.

■ ASSOCIATED CONTENT

Ⓢ Supporting Information

Supplementary Figure S1 showing the fully optimized S-VWN/SDD geometry of the $[Zn_2{\cdot}(SC_2H_5)_6]^{2-}$ complex; Supplementary Table S1 comparing the computed and X-ray distances and angles in the $[Zn_2{\cdot}(SC_2H_5)_6]^{2-}$ complex using various methods; Supplementary Tables S2a and S2b listing hydrogen bonds present in the X-ray structures and MD simulations, respectively. Supplementary Tables S3a and S3b listing the QM/MM energies, electrostatic solvation free energies, and solvent accessible surface areas of 36 frames from the 4.5−22 ns MD trajectories of the reactant and product states of the β and α domain, respectively. This material is available free of charge via the Internet at http://pubs.acs.org.

■ AUTHOR INFORMATION

Corresponding Author

*E-mail: carmay@gate.sinica.edu.tw; Tel: 886-2-2652-3031.

Present Address

[§]Faculty of Chemistry and Pharmacy, Sofia University, Sofia 1164, Bulgaria.

Author Contributions

[‖]Equal contribution.

Notes

The authors declare no competing financial interest.

■ ACKNOWLEDGMENTS

We thank Drs. Jon Wright and Qiang Cui for help with CHARMM37-GAUSSIAN09 interface. This work was supported by Academia Sinica and the Ministry of Science & Technology (NSC-98-2113-M-001-011) Taiwan and EU Grant "Beyond Everest", FP7-REGPOT-2011-1.

■ REFERENCES

(1) Bell, S. G.; Vallee, B. L. The Metallothionein/Thionein System: An Oxidoreductive Metabolic Zinc Link. *ChemBioChem* **2009**, *10*, 55−62.

(2) Maret, W.; Li, Y. Coordination Dynamics of Zinc in Proteins. *Chem. Rev.* **2009**, *109*, 4682−4707.

(3) Hartmann, H. J.; Weser, U. Copper-Thionein from Fetal Bovine Liver. *Biochim. Biophys. Acta* **1977**, *491*, 211−222.

(4) Ryden, L.; Deutsch, H. F. Preparation and Properties of Major Copper-Binding Component in Human Fetal Liver - Its Identification as Metallothionein. *J. Biol. Chem.* **1978**, *253*, 519−524.

(5) Masters, B. A.; Quaife, C. J.; Erickson, J. C.; Kelly, E. J.; Froelick, G. J.; Zambrowicz, B. P.; Brinster, R. L.; Palmiter, R. D. Metallothionein-III Is Expressed in Neurons That Sequester Zinc in Synaptic Vesicles. *J. Neurosci.* **1994**, *14*, 5844−5857.

(6) Uchida, Y.; Takio, K.; Titani, K.; Ihara, Y.; Tomonaga, M. The Growth Inhibitory Factor That Is Deficient in the Alzheimers-Disease Brain Is a 68-Amino Acid Metallothionein-Like Protein. *Neuron* **1991**, *7*, 337−347.

(7) Quaife, C. J.; Findley, S. D.; Erickson, J. C.; Froelick, G. J.; Kelly, E. J.; Zambrowicz, B. P.; Palmiter, R. D. Induction of a New Metallothionein Isoform (MT-IV) Occurs during Differentiation of Stratified Squamous Epithelia. *Biochemistry* **1994**, *33*, 7250−7259.

(8) Li, Y.; Maret, W. Human metallothionein metallomics. *J. Anal. At. Spectrom.* **2008**, *23*, 1055−1062.

(9) Bremner, I.; Beattie, J. H. Metallothionein and the Trace Minerals. *Annu. Rev. Nutr.* **1990**, *10*, 63−83.

(10) Schwarz, M. A.; Lazo, J. S.; Yalowich, J. C.; Allen, W. P.; Whitmore, M.; Bergonia, H. A.; Tzeng, E.; Billiar, T. R.; Robbins, P. D.; Lancaster, J. R.; et al. Metallothionein Protects against the Cytotoxic and DNA-Damaging Effects of Nitric-Oxide. *Proc. Natl. Acad. Sci. U.S.A.* **1995**, *92*, 4452−4456.

(11) Palmiter, R. D. The elusive function of metallothioneins. *Proc. Natl. Acad. Sci. U. S. A.* **1998**, *95*, 8428−8430.

(12) Miles, A. T.; Hawksworth, G. M.; Beattie, J. H.; Rodilla, V. Induction, regulation, degradation, and biological significance of mammalian metallothioneins. *Crit. Rev. Biochem. Mol. Biol.* **2000**, *35*, 35−70.

(13) Hidalgo, J.; Aschner, M.; Zatta, P.; Vašák, M. Roles of the metallothionein family of proteins in the central nervous system. *Brain Res. Bull.* **2001**, *55*, 133−145.
(14) Coyle, P.; Philcox, J. C.; Carey, L. C.; Rofe, A. M. Metallothionein: The multipurpose protein. *Cell. Mol. Life Sci.* **2002**, *59*, 627−647.
(15) Maret, W. New perspectives of zinc coordination environments in proteins. *J. Inorg. Biochem.* **2012**, *111*, 110−116.
(16) Suhy, D. A.; Simon, K. D.; Linzer, D. I. H.; O'Halloran, T. V. Metallothionein is part of a zinc-scavenging mechanism for cell survival under conditions of extreme zinc deprivation. *J. Biol. Chem.* **1999**, *274*, 9183−9192.
(17) Outten, C. E.; O'Halloran, T. V. Femtomolar sensitivity of metalloregulatory proteins controlling zinc homeostasis. *Science* **2001**, *292*, 2488−2492.
(18) Krezel, A.; Hao, Q.; Maret, W. Zinc/thiolate redox biochemistry of metallothionein and the control of zinc ion fluctuations in cell signaling. *Arch. Biochem. Biophys.* **2007**, *463*, 188−200.
(19) Maret, W. Zinc and sulfur: A critical biological partnership. *Biochemistry* **2004**, *43*, 3301−3309.
(20) Jacob, C.; Maret, W.; Vallee, B. L. Control of zinc transfer between thionein, metallothionein, and zinc proteins. *Proc. Natl. Acad. Sci. U. S. A.* **1998**, *95*, 3489−3494.
(21) Capdevila, M.; Bofill, R.; Palacios, O.; Atrian, S. State-of-the-art of metallothioneins at the beginning of the 21st century. *Coord. Chem. Rev.* **2012**, *256*, 46−62.
(22) Ruttkay-Nedecky, B.; Nejdl, L.; Gumulec, J.; Zitka, O.; Masarik, M.; Eckschlager, T.; Stiborova, M.; Adam, V.; Kizek, R. The Role of Metallothionein in Oxidative Stress. *Int. J. Mol. Sci.* **2013**, *14*, 6044−6066.
(23) Jin, G. B.; Inoue, S.; Urano, T.; Cho, S.; Ouchi, Y.; Cyong, J. C. Induction of anti-metallothionein antibody and mercury treatment decreases bone mineral density in mice. *Toxicol. Appl. Pharmacol.* **2002**, *185*, 98−110.
(24) Cherian, M. G.; Jayasurya, A.; Bay, B. H. Metallothioneins in human tumors and potential roles in carcinogenesis. *Mutat. Res.* **2003**, *533*, 201−209.
(25) Kartalou, M.; Essigmann, J. M. Mechanisms of resistance to cisplatin. *Mutat. Res.* **2001**, *478*, 23−43.
(26) Knipp, M. Metallothioneins and Platinum(II) Anti-Tumor Compounds. *Curr. Med. Chem.* **2009**, *16*, 522−537.
(27) Durand, J.; Meloni, G.; Talmard, C.; Vašák, M.; Faller, P. Zinc release of Zn-7-metallothionein-3 induces fibrillar type amyloid-β aggregates. *Metallomics* **2010**, *2*, 741−744.
(28) Kepp, K. P. Bioinorganic Chemistry of Alzheimer's Disease. *Chem. Rev.* **2012**, *112*, 5193−5239.
(29) Islam, M. S.; Loots, D. T. Diabetes, metallothionein, and zinc interactions: A review. *Biofactors* **2007**, *29*, 203−212.
(30) Pedersen, M. O.; Larsen, A.; Stoltenberg, M.; Penkowa, M. The role of metallothionein in oncogenesis and cancer prognosis. *Prog. Histochem. Cytochem.* **2009**, *44*, 29−64.
(31) Vašák, M.; Meloni, G. Chemistry and biology of mammalian metallothioneins. *J. Biol. Inorg. Chem.* **2011**, *16*, 1067−1078.
(32) Braun, W.; Vašák, M.; Robbins, A. H.; Stout, C. D.; Wagner, G.; Kagi, J. H. R.; Wuthrich, K. Comparison of the NMR Solution Structure and the X-ray Crystal-Structure of Rat Metallothionein-2. *Proc. Natl. Acad. Sci. U. S. A.* **1992**, *89*, 10124−10128.
(33) Jiang, L. J.; Vašák, M.; Vallee, B. L.; Maret, W. Zinc transfer potentials of the alpha- and beta-clusters of metallothionein are affected by domain interactions in the whole molecule. *Proc. Natl. Acad. Sci. U.S.A.* **2000**, *97*, 2503−2508.
(34) Oz, G.; Zangger, K.; Armitage, I. M. Three-dimensional structure and dynamics of a brain specific growth inhibitory factor: Metallothionein-3. *Biochemistry* **2001**, *40*, 11433−11441.
(35) Blindauer, C. A.; Harrison, M. D.; Parkinson, J. A.; Robinson, A. K.; Cavet, J. S.; Robinson, N. J.; Sadler, P. J. A metallothionein containing a zinc finger within a four-metal cluster protects a bacterium from zinc toxicity. *Proc. Natl. Acad. Sci. U. S. A.* **2001**, *98*, 9593−9598.
(36) Munoz, A.; Forsterling, F. H.; Shaw, C. F.; Petering, D. H. Structure of the $^{113}Cd_3$ β domains from Homarus americanus metallothionein-1: Hydrogen bonding and solvent accessibility of sulfur atoms. *J. Biol. Inorg. Chem.* **2002**, *7*, 713−724.
(37) Blindauer, C. A.; Sadler, P. J. How to hide zinc in a small protein. *Acc. Chem. Res.* **2005**, *38*, 62−69.
(38) Blindauer, C. A.; Leszczyszyn, O. I. Metallothioneins: Unparalleled diversity in structures and functions for metal ion homeostasis and more. *Nat. Prod. Rep.* **2010**, *27*, 720−741.
(39) Jensen, K. P.; Rykaer, M. The building blocks of metallothioneins: Heterometallic Zn^{2+} and Cd^{2+} clusters from first-principles calculations. *Dalton Trans.* **2010**, *39*, 9684−9695.
(40) Kepp, K. P. Full quantum-mechanical structure of the human protein Metallothionein-2. *J. Inorg. Biochem.* **2012**, *107*, 15−24.
(41) Kassim, R.; Ramseyer, C.; Enescu, M. Oxidation reactivity of zinc-cysteine clusters in metallothionein. *J. Biol. Inorg. Chem.* **2013**, *18*, 333−342.
(42) Rigby, K. E.; Chan, J.; Mackie, J.; Stillman, M. J. Molecular dynamics study on the folding and metallation of the individual domains of metallothionein. *Proteins: Struct., Funct., Bioinf.* **2006**, *62*, 159−172.
(43) Berweger, C. D.; Thiel, W.; van Gunsteren, W. F. Molecular-dynamics simulation of the beta domain of metallothionein with a semi-empirical treatment of the metal core. *Proteins: Struct., Funct., Bioinf.* **2000**, *41*, 299−315.
(44) Ni, F. Y.; Cai, B.; Ding, Z. C.; Zheng, F.; Zhang, M. J.; Wu, H. M.; Sun, H. Z.; Huang, Z. X. Structural prediction of the beta-domain of metallothionein-3 by molecular dynamics simulation. *Proteins: Struct., Funct., Bioinf.* **2007**, *68*, 255−266.
(45) Romero-Isart, N.; Oliva, B.; Vašák, M. Influence of NH - S^{γ} bonding interactions on the structure and dynamics of metallothioneins. *J. Mol. Model.* **2010**, *16*, 387−394.
(46) Sakharov, D. V.; Lim, C. Zn protein simulations including charge transfer and local polarization effects. *J. Am. Chem. Soc.* **2005**, *127*, 4921−4929.
(47) Babu, C. S.; Lim, C. Empirical force fields for biologically active divalent metal cations in water. *J. Phys. Chem. A* **2006**, *110*, 691−699.
(48) Sakharov, D. V.; Lim, C. Force Fields Including Charge Transfer and Local Polarization Effects: Application to Proteins Containing Multi/Heavy Metal Ions. *J. Comput. Chem.* **2009**, *30*, 191−202.
(49) Krezel, A.; Maret, W. Dual nanomolar and picomolar Zn(II) binding properties of metallothionein. *J. Am. Chem. Soc.* **2007**, *129*, 10911−10921.
(50) Jiang, L. J.; Maret, W.; Vallee, B. L. The glutathione redox couple modulates zinc transfer from metallothionein to zinc-depleted sorbitol dehydrogenase. *Proc. Natl. Acad. Sci. U. S. A.* **1998**, *95*, 3483−3488.
(51) Korichneva, I.; Hoyos, B.; Chua, R.; Levi, E.; Hammerling, U. Zinc release from protein kinase C as the common event during activation by lipid second messenger or reactive oxygen. *J. Biol. Chem.* **2002**, *277*, 44327−44331.
(52) Allen, F. H. The Cambridge Structural Database: A quarter of a million crystal structures and rising. *Acta Crystallogr., Sect. B: Struct. Sci.* **2002**, *58*, 380−388.
(53) Watson, A. D.; Rao, C. P.; Dorfman, J. R.; Holm, R. H. Systematic Stereochemistry of Metal(II) Thiolates - Synthesis and Structures of $[Mn(II)_2(SC_2H_5)_6]^{2-}$, $[Ni(II)_2(SC_2H_5)_6]^{2-}$, $[Zn(II)_2(SC_2H_5)_6]^{2-}$, $[Cd(II)_2(SC_2H_5)_6]^{2-}$. *Inorg. Chem.* **1985**, *24*, 2820−2826.
(54) Frisch, M. J.; Trucks, G. W.; Schlegel, H. B.; Scuseria, G. E.; Robb, M. A.; Cheeseman, J. R.; Scalmani, G.; Barone, V.; Mennucci, B.; Petersson, G. A., et al. *Gaussian 09*, revision A.02, Gaussian, Inc.: Wallingford CT, 2009.
(55) Luber, S.; Reiher, M. Theoretical Raman Optical Activity Study of the β Domain of Rat Metallothionein. *J. Phys. Chem. B* **2010**, *114*, 1057−1063.
(56) Ohanessian, G.; Picot, D.; Frison, G. Reactivity of Polynuclear Zinc-Thiolate Sites. *Int. J. Quantum Chem.* **2011**, *111*, 1239−1247.

(57) Greisen, P.; Jespersen, J. B.; Kepp, K. P. Metallothionein Zn^{2+}- and Cu^{2+}-clusters from first-principles calculations. *Dalton Trans.* **2012**, *41*, 2247−2256.
(58) Brooks, B. R.; Brooks, C. L.; Mackerell, A. D.; Nilsson, L.; Petrella, R. J.; Roux, B.; Won, Y.; Archontis, G.; Bartels, C.; Boresch, S.; et al. CHARMM: The Biomolecular Simulation Program. *J. Comput. Chem.* **2009**, *30*, 1545−1614.
(59) MacKerell, A. D.; Bashford, D.; Bellott, M.; Dunbrack, R. L.; Evanseck, J. D.; Field, M. J.; Fischer, S.; Gao, J.; Guo, H.; Ha, S.; et al. All-atom empirical potential for molecular modeling and dynamics studies of proteins. *J. Phys. Chem. B* **1998**, *102*, 3586−3616.
(60) Jorgensen, W. L.; Chandrasekhar, J.; Madura, J. D.; Impey, R. W.; Klein, M. L. Comparison of Simple Potential Functions for Simulating Liquid Water. *J. Chem. Phys.* **1983**, *79*, 926−935.
(61) Ryckaert, J. P.; Ciccotti, G.; Berendsen, H. J. C. Numerical-Integration of Cartesian Equations of Motion of a System with Constraints - Molecular-Dynamics of N-Alkanes. *J. Comput. Phys.* **1977**, *23*, 327−341.
(62) Darden, T.; York, D.; Pedersen, L. Particle Mesh Ewald - An *N*·log(*N*) Method for Ewald Sums in Large Systems. *J. Chem. Phys.* **1993**, *98*, 10089−10092.
(63) Singh, U. C.; Kollman, P. A. An Approach to Computing Electrostatic Charges for Molecules. *J. Comput. Chem.* **1984**, *5*, 129−145.
(64) Field, M. J.; Bash, P. A.; Karplus, M. A Combined Quantum-Mechanical and Molecular Mechanical Potential for Molecular-Dynamics Simulations. *J. Comput. Chem.* **1990**, *11*, 700−733.
(65) Woodcock, H. L.; Hodoscek, M.; Gilbert, A. T. B.; Gill, P. M. W.; Schaefer, H. F.; Brooks, B. R. Interfacing Q-chem and CHARMM to perform QM/MM reaction path calculations. *J. Comput. Chem.* **2007**, *28*, 1485−1502.
(66) Dudev, T.; Lim, C. All-electron calculations of the nucleation structures in metal-induced zinc-finger folding: Role of the peptide backbone. *J. Am. Chem. Soc.* **2007**, *129*, 12497−12504.
(67) Nina, M.; Im, W.; Roux, B. Optimized atomic radii for protein continuum electrostatics solvation forces. *Biophys. Chem.* **1999**, *78*, 89−96.
(68) Rizzo, R. C.; Aynechi, T.; Case, D. A.; Kuntz, I. D. Estimation of absolute free energies of hydration using continuum methods: Accuracy of partial charge models and optimization of nonpolar contributions. *J. Chem. Theory Comput.* **2006**, *2*, 128−139.
(69) Lee, Y. M.; Lim, C. Factors Controlling the Reactivity of Zinc Finger Cores. *J. Am. Chem. Soc.* **2011**, *133*, 8691−8703.
(70) Lee, Y. M.; Lim, C. Physical basis of structural and catalytic Zn-binding sites in proteins. *J. Mol. Biol.* **2008**, *379*, 545−553.
(71) Lin, Y. L.; Lim, C. Factors governing the protonation state of Zn-bound histidine in proteins: A DFT/CDM study. *J. Am. Chem. Soc.* **2004**, *126*, 2602−2612.
(72) Vosko, S. H.; Wilk, L.; Nusair, M. Accurate Spin-Dependent Electron Liquid Correlation Energies for Local Spin-Density Calculations - A Critical Analysis. *Can. J. Phys.* **1980**, *58*, 1200−1211.
(73) Andrae, D.; Haussermann, U.; Dolg, M.; Stoll, H.; Preuss, H. Energy-Adjusted Ab Initio Pseudopotentials for the 2nd and 3rd Row Transition-Elements. *Theor. Chim. Acta* **1990**, *77*, 123−141.